

Timing Acquisition and Error Analysis for Pulse-Based Terahertz Band Wireless Systems

Chong Han, *Member, IEEE*, Ian F. Akyildiz, *Fellow, IEEE*, and Wolfgang H. Gerstacker, *Senior Member, IEEE*

Abstract—Terahertz (THz) band communication is envisioned as a key technology to satisfy the increasing demand for ultra-broadband wireless systems, thanks to its ultrabroad bandwidth. Tailored for the unique properties of pulse-based communications in the THz band, two timing acquisition algorithms are proposed and analyzed thoroughly in this paper. First, a low-sampling-rate (LSR) synchronization algorithm is proposed, by extending the theory of sampling signals with finite rate of innovation in the communication context and exploiting the properties of the annihilating filter. The simulation results show that the timing accuracy at an order of ten picoseconds is achievable. In particular, the LSR algorithm has high performance with uniform sampling at 1/20 of the Nyquist rate when the signal-to-noise ratio (SNR) is high (i.e., greater than 18 dB). Complementary to this, a maximum likelihood (ML) approach for timing acquisition is developed, which searches for the timing offsets by adopting a two-step acquisition procedure based on the ML criterion. The simulation results show that the ML-based algorithm is well suitable in the low SNR case with a half-reduced search space. For further evaluation, the error performance and the resulting bit-error-rate sensitivity to the timing errors in the LSR and the ML algorithms are both analytically and numerically studied. This paper provides very different and promising angles to efficiently and reliably solve the timing acquisition problem for pulse-based THz band wireless systems.

Index Terms—Terahertz band, timing acquisition, synchronization, low-sampling-rate, maximum likelihood approach.

I. INTRODUCTION

IN RECENT years, the wireless data traffic grew exponentially, further accompanied by an increasing demand for higher data rates. The data rates have doubled every eighteen months over the last three decades and are currently approaching the capacity of communication systems [1]. The (0.06–10) Terahertz band is identified as one of the promising spectrum

bands to address the spectrum scarcity and capacity limitations of current wireless systems [2]. The main benefit of the THz band comes from its ultra-broad bandwidth, which ranges from tens of GHz up to a few THz [3]. The use of this frequency band is envisioned to enable ultra-high-speed wireless communications, and boost a plethora of applications [4].

The huge bandwidth of the THz band comes at costs. First, a highly frequency- and distance-selective path loss, which causes severe distortion, including attenuation and temporal broadening effects, on the transmitted pulses [5]. Second, the digital synchronization, which has the advantages of cost-efficiency, full integration, and robustness [6], [7], requires multi-hundreds-Giga-samples-per-second (Gs/s) and even Tera-samples-per-second (Ts/s) sampling rates, while the fastest sampling rate to date does not exceed 100 Gs/s [8], [9]. Due to these reasons, timing errors as small as picoseconds can seriously degrade the system performance. As a result, timing acquisition, which is one part of the synchronization, constitutes an important but yet fully unexplored topic in the THz band system design to date.

To address the aforementioned challenges, two timing acquisition algorithms are proposed and evaluated for pulse-based THz band communications in this paper. First, in order to achieve efficient timing acquisition with reduced sampling rates, we extend the theory of sampling signals with finite rate of innovation [10]–[13] from compressive sampling in signal processing to the communication context. The first focus of this work is that we propose a *low-sampling-rate (LSR) algorithm* for timing acquisition in the THz band. In our LSR algorithm, we leverage the features of the annihilating filters which have been introduced in [14], [15] and apply them in the context of THz pulse-based communications. Moreover, we investigate the LSR algorithm in the THz band by considering the communication parameters, which include the antenna gain, the distance, the number of frames per symbol and the pulse width. However, the proposed LSR works well when the signal-to-noise ratio (SNR) is high and appears to be not suitable when the SNR is below 18 dB [16]. Therefore, the second focus of this work is that a *maximum likelihood (ML) approach* for timing acquisition is proposed in the low SNR case for THz band communications, complementary to the LSR approach. This algorithm adopts a two-step acquisition procedure to derive the timing acquisition solutions based on the ML criterion [17]–[19].

Furthermore, we analytically and numerically evaluate the LSR and the ML timing acquisition algorithms, in comparison with the Cramer-Rao lower bound (CRLB). In addition, we perform an analysis on the bit-error-rate (BER) sensitivity to the acquisition errors for the two algorithms. Then, extensive evaluations on the performance of the proposed two approaches are carried out via simulations, with the variation of the THz communication parameters, including the antenna gain, the distance,

Manuscript received April 9, 2017; revised August 2, 2017; accepted September 6, 2017. Date of publication September 11, 2017; date of current version November 10, 2017. This work was supported in part by the U.S. National Science Foundation under Grant ECCS-1608579, and in part by the Alexander von Humboldt Foundation through Prof. Akyildiz's Humboldt Research Prize in Germany. The review of this paper was coordinated by Prof. S.-H. Leung. (*Corresponding author: Chong Han.*)

C. Han is with the University of Michigan–Shanghai Jiao Tong University Joint Institute, Shanghai Jiao Tong University, Shanghai 200240, China (e-mail: chong.han@sjtu.edu.cn).

I. F. Akyildiz is with the Broadband Wireless Networking Laboratory, School of Electrical and Computer Engineering, Georgia Institute of Technology, Atlanta, GA 30332 USA (e-mail: ian@ece.gatech.edu).

W. H. Gerstacker is with the Institute for Digital Communications, Friedrich-Alexander-University Erlangen-Nuernberg, Erlangen 91058, Germany (e-mail: gersta@LNT.de).

Color versions of one or more of the figures in this paper are available online at <http://ieeexplore.ieee.org>.

Digital Object Identifier 10.1109/TVT.2017.2750707

the symbol rate and the pulse width. The simulation results show that the timing accuracy at an order of ten picoseconds is achievable. In particular, the LSR algorithm performs well for a uniform sampling at 1/20 of the Nyquist rate with a high SNR, while the ML approach is well suitable in the low SNR case and supports a half-reduced search space. Our paper contributes to achieving the efficient and reliable timing acquisition for THz band wireless systems.

The rest of this paper is organized as follows. The related work is reviewed in Section II. In Section III, we provide the channel and the signal model for THz band communications. We proceed to delineate the LSR synchronization algorithm in Section IV. The timing acquisition solutions based on the ML criterion are derived in Section V. The performances of the two approaches are compared with the CRLB in Section VI, and the analysis of the BER sensitivity to the timing errors is provided. In Section VII, extensive performance evaluations are presented. Finally, we conclude the paper in Section VIII.

II. RELATED WORK

To the best of our knowledge, only a few timing acquisition solutions have been proposed for THz systems so far. In [20], a non-coherent receiver architecture based on a continuous-time moving average symbol detection scheme is introduced for the THz pulse-based communication. Although this scheme does not require the Nyquist sampling rate [21], the symbol start time needs to be iteratively determined. Furthermore, the threshold value used in this detection-based approach is not analytically provided and hence, the accuracy of the timing estimation is not guaranteed.

Instead, we propose LSR and ML based timing acquisition algorithms, which provide different and promising approaches to solve the timing acquisition problem in the THz band. Although these two methods were previously used for lower frequencies systems, they cannot be directly applied to the THz systems. On the one hand, the sub-Nyquist sampling rate was firstly proposed for compressive sensing for signal reconstruction [11]. This idea was then adopted for ultra-wideband (UWB) systems [22]. On the other hand, the ML method is commonly used for signal detection, channel estimation, and synchronization [23].

However, the channel peculiarities in the THz band such as the molecular absorption loss and the temporal broadening effect make the THz spectrum drastically distance- and frequency-selective. These effects substantially distort the THz transmission, and largely differentiate from the effects in wireless systems at lower frequencies. Therefore, they need to be carefully treated in analyzing the timing acquisition problem. Moreover, the pulse duration of THz communication is at the order of pico-seconds, which is over three orders of magnitude lower than that in lower-frequency systems, such as impulse-radio UWB [24]. This significantly increases the challenges in timing acquisition.

Additionally, the broad bandwidth of THz band signaling ranges from tens of GHz up to several THz, which significantly increases the difficulties of synchronization. For example, the authors in [25] suggest a sampling rate of one fourth of the Nyquist rate for the UWB system. Nevertheless, owing to the very broad bandwidth of the THz spectrum, this sampling rate is still too high and needs to be further reduced. An alternative way based on time-interleaved ADC system has been proposed, in which several channel ADCs operate at interleaved

sampling times as if they were effectively a single ADC operating at a much higher sampling rate. However, not only the additional circuit size and power consumption, but also the offset mismatches, gain mismatches among channel ADCs as well as timing skew of the clocks limit the feasibility of this approach for mobile wireless devices [26]. Last but not least, the varying THz communication parameters, including the antenna gain, the distance, the symbol rate and the pulse width, need to be jointly incorporated in the performance evaluation for the two timing acquisition algorithms.

This paper is an extension of our preliminary study in [16], with much more details in the LSR and ML algorithms, as well as more thoroughly investigation on their performance evaluations. In addition, the error performance and the resulting BER sensitivity to the timing errors of two proposed algorithms are analytically and numerically studied and included in this work.

III. TERAHERTZ BAND CHANNEL AND PULSE-BASED WAVEFORM MODEL

In this section, we introduce the THz channel model and describe the pulse-based waveform design. Then, we precisely define the timing acquisition problem in this framework.

A. Overview of Terahertz Band Channel

The channel impulse response $h(t)$ of the THz band channel is obtained by applying the inverse Fourier transform to the transfer function $H(f)$,

$$h(t) = \sqrt{G_t G_r} \cdot \mathcal{F}^{-1} \{H(f)\}, \quad (1)$$

where G_t and G_r denote the transmit and receive antenna gains. Thanks to the very small wavelength at THz frequencies, very large antenna arrays could be packed to enable beamforming and directional gain [4]. The resulting gain could reach 30 dB [2], [16]. The inverse Fourier Transform in (1) does not have an analytical expression. In our analysis, we will numerically compute the channel impulse response.

Then, the channel frequency response for the THz wave propagation in (1) is given by

$$H(f) = \frac{c}{4\pi f d_T} \cdot \exp\left(-\frac{1}{2}\mathcal{K}(f)d_T\right), \quad (2)$$

where c stands for the speed of light, f is the operating frequency, and d_T represents the total traveling distance. The molecular absorption coefficient, $\mathcal{K}(f)$, is frequency-selective and accounts for the attenuation resulting from the fact that part of the wave energy is converted into internal kinetic energy of the molecules in the propagation medium [27].

From Fig. 1, we characterize the channel in terms of the distance-varying spectral windows, and the temporal broadening effects. First, the path loss peaks caused by the molecular absorption create spectral windows, which have different bandwidth and drastically change with the distance. For example, a few path loss peaks appear between 0.06 to 1 THz for $d_T = 1, 5, 10, 30$ m, such as at 0.56 THz, 0.75 THz, and 0.98 THz. The number of peaks increases with the distance. Second, this strong frequency-selectivity causes the temporal broadening effect [5], which restricts the minimum spacing between the consecutive signaling and results in a coherence bandwidth, regardless of the multipath delay spread. As a result, these unique channel properties in the THz band complicate the task of

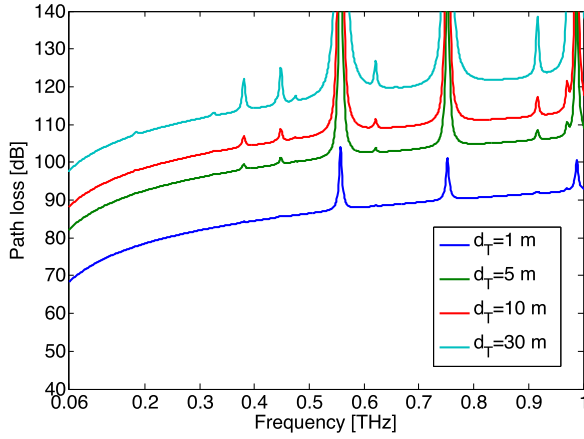


Fig. 1. Path loss of the THz band channel. $G_t = G_r = 0$ dB.

synchronization. Furthermore, the performance of the proposed timing acquisition solutions will need to be evaluated under the varying THz communication parameters, including the antenna gain, the distance, and the pulse modulation.

B. Terahertz Pulse Waveform and Timing Offsets

In [28], a wideband pulse waveform is proposed for the THz band communication. The data rate could reach 30 Gbps over 20 m, using the wideband pulse waveform combined with directional transmissions. In particular, an ultra-short Gaussian pulse is proposed for THz band communications. The pulse duration is $T_p = 10$ ps. For pulse-based THz communication, every information symbol consists of N_f repeated pulses (i.e., one pulse in one frame while multiple frames constitute one symbol), which creates a pulse combining gain to improve the SNR at the receiver. The transmit signal, $s(t)$, is expressed as

$$s(t) = \sqrt{P_t} \sum_{i=0}^{I-1} a_i \sum_{k=0}^{N_f-1} p(t - iN_f T_f - kT_f - \tau_0), \quad (3)$$

where $a_i \in \{+1, -1\}$ refers to the i th binary information symbol, I is the total number of symbols. N_f denotes the number of pulse waveforms or frames to represent one symbol, and T_f is the time duration of a frame. Moreover, P_t represents the transmit power, k is the index of the pulses corresponding to one symbol. The resulting transmit and receive signals are shown in Fig. 2, with $I = 1$ and $N_f = 3$. Moreover, τ_0 stands for the random initial transmission delay. $p(t)$ is the wideband transmit pulse with the duration T_p and a unit energy.

The received signal including the THz channel effects is

$$\begin{aligned} y(t) &= s(t) * h(t) + w(t) \\ &= \sqrt{P_t} \sum_{i=0}^{I-1} a_i \sum_{k=0}^{N_f-1} g(t - iN_f T_f - kT_f - \tau_0 - t_D - \psi_i) + w(t) \\ &= \sqrt{P_t} \sum_{i=0}^{I-1} a_i \sum_{k=0}^{N_f-1} g(t - iN_f T_f - kT_f - \mu_i T_f - \nu_i T_s) + w(t) \end{aligned} \quad (4)$$

where $w(t)$ is the white Gaussian noise, and $g(t)$ represents the received pulse of $p(t)$ in (3) through the THz channel. Moreover,

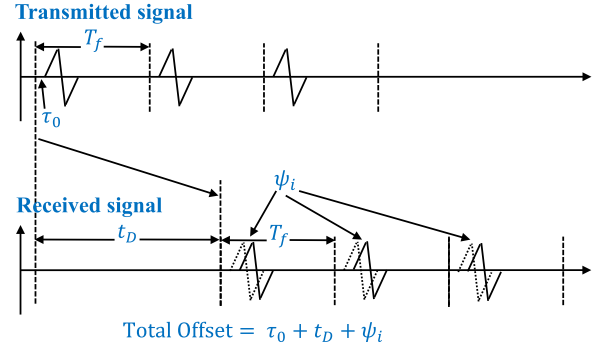


Fig. 2. A pulse-based Terahertz transmit and received signal, with $I = 1$ and $N_f = 3$. The timing offsets are shown, which include the random starting time τ_0 , the propagation delay t_D , and the jittering offset ψ_i .

the sampling interval is defined as the inverse of the sampling rate,

$$T_s = \frac{1}{N_s} = \frac{\beta_{LSR}}{N_{ny}}, \quad (5)$$

where the sampling interval is the smallest time interval considered in the digital timing acquisition system. Therefore, the timing offsets are integer multiples of T_s . Furthermore, the integer value Q denotes the number of samples per frame that relates the sampling interval T_s and the frame duration T_f , as $T_s = T_f/Q$. Then, any time duration can be represented as $\mu_i T_f + \nu_i T_s$, in which ν_i takes integer values in the range of $[0, Q - 1]$ and the multiple of T_f is absorbed in the integer parameter μ_i .

In terms of the delays, $t_D = d_T/c$ stands for the transmission delay, and ψ_i denotes the jittering offset or the random misalignment between the transmitter and receiver clocks, which dynamically varies over symbols. This consideration is reasonable since the pulse duration is at the order of pico-seconds in the pulse-based THz communications. Then, the timing offsets in (4) are given by

$$\mu_i T_f + \nu_i T_s = \tau_0 + t_D + \psi_i. \quad (6)$$

where μ_i identifies the first frame of a symbol that amounts to the symbol timing (ST) at the frame level. This parameter suggests the symbol begins at $t = iN_f T_f + \mu_i T_f$. On the other hand, ν_i indicates the frame timing (FT) at the sample level, and suggests the frame begins at $t = (iN_f + k + \mu_i) T_f + \nu_i T_s$.

As shown in Fig. 2, the timing acquisition for the THz band communication accounts for the offsets that include the following three parts: i) the random starting time, τ_0 , ii) the propagation delay, t_D , which is a constant if the transmitter and the receiver are fixed, and iii) the jittering offset, ψ_i , which is different for the different symbols. Equivalently, the problem of timing acquisition becomes solving for μ_i and ν_i .

Based on the received signal in (4) and the channel response in (1), the SNR is calculated as

$$\gamma = \frac{G_t G_r P_t N_f \int_0^{T_f} |h(t)|^2 dt}{P_w}, \quad (7)$$

where P_w refers to the noise power of $w(t)$ in (4) within the transmission band. As the number of pulses per symbol N_f increases, the SNR increases and consequently, the synchronization performance will improve. However, this is at the cost of the sacrifice of data rates. Furthermore, the antenna gains and

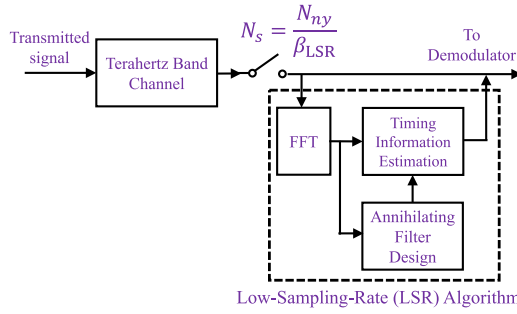


Fig. 3. Block diagram of the LSR algorithm.

the communication distance have the influences on the SNR as well. Therefore, there is a tradeoff among the SNR, the synchronization performance, and the data rate, which needs to be carefully treated in the THz wireless system design.

IV. LOW-SAMPLING-RATE (LSR) ALGORITHM FOR TIMING ACQUISITION

In this section we will show that it is possible to reliably decode a received signal by sampling it at or above the rate of innovation, not at the sampling rate dictated by the bandwidth of the transmit signal. This approach was adopted for ultra-wideband (UWB) systems [22], [25]. In this section, we tailor the algorithm to the THz band to cope with the unique THz channel characteristics and the more challenging requirement for the reduction of the sampling rate.

Based on the annihilating filter method and the spectral estimation techniques in the frequency domain, the resulting LSR algorithm can estimate the timing information at a sub-Nyquist rate. In particular, the annihilating filter method is a well-known tool from the spectral estimation [14], [15], [29], [30], while in our context, we derive the analytical sampling formulas in the THz band. The flow of the LSR algorithm for the timing acquisition is described in Fig. 3, and consists of the three steps, namely, 1) computing the spectral coefficients, 2) designing the annihilating filter, and 3) determining the timing offsets. Moreover, we define the *LSR factor* as the ratio between the Nyquist sampling rate N_{ny} , and the implemented sampling rate N_s , i.e., $\beta_{LSR} = N_{ny}/N_s$. In the following, we detail the three steps of the LSR algorithm.

A. Computing the Spectral Coefficients

By performing the Fourier transform on the received signal in (4), the equivalent signal model in the frequency domain is

$$Y(f) = \sqrt{P_t} \sum_{i=0}^{I-1} a_i \sum_{k=0}^{N_f-1} \sqrt{G_t G_r} \frac{c}{4\pi f d_T} \exp\left(-\frac{1}{2}\mathcal{K}(f)d_T\right) \cdot P(f) \exp(-j2\pi f (iN_f T_f + kT_f)) \cdot \exp(-j2\pi f (\mu_i T_f + \nu_i T_s)) + W(f), \quad (8)$$

where $P(f)$ and $W(f)$ represent the frequency responses of $p(t)$ and $w(t)$, in (3) and (4). After sampling at the rate N_s , the discrete-time signal of (4) becomes

$$y[n] = \sqrt{P_t} \sum_{i=0}^{I-1} a_i \sum_{k=0}^{N_f-1} g[n - iN_f Q - kQ - \mu_i Q - \nu_i] + w[n]. \quad (9)$$

Next, we transform the signals into the discrete frequency domain. If the specific THz band with the upper and lower cutoff frequencies of f_U and f_L are selected, the frequency step is defined as $f_0 = \frac{f_U - f_L}{N}$. In the frequency domain, the N uniformly spaced frequency samples can be expressed as

$$Y[n] = \sum_{i=0}^{I-1} A_i[n] \sum_{k=0}^{N_f-1} \exp(-j2\pi f_n (iN_f T_f + kT_f)) \cdot \exp(-j2\pi f_n (\mu_i T_f + \nu_i T_s)) + W[n] \\ = \sum_{i=0}^{I-1} \sum_{k=0}^{N_f-1} A_i[n] u_{i,k}^n + W[n], \quad n = 0, 1, \dots, N-1 \quad (10)$$

where $f_n = f_L + n f_0$. In the above equations, the expanded expressions for $A_i[n]$ and $u_{i,k}^n$ are given by

$$A_i[n] = a_i \sqrt{G_t G_r P_t} \frac{c}{4\pi f_n d_T} e^{-\frac{1}{2}\mathcal{K}(f_n)d_T} P(f_n), \quad (11)$$

$$u_{i,k}^n = e^{(-j2\pi f_n T_f (iN_f + k + \mu_i)) + (-j2\pi f_n T_s \nu_i)}. \quad (12)$$

Note that $u_{i,k}^n$ depends on i and k .

As a preparation for invoking the annihilating filter-based LSR algorithm, the coefficients $A_i[n]$ in (11), which depend on the transmitted symbol, antenna gains, transmit power, THz channel attenuation and distortion, are approximated in a polynomial function, as a sum of powers with the exponents of $m \in [0, M-1]$,

$$A_i[n] \approx \sum_{m=0}^{M-1} x_m n^m, \quad (13)$$

where x_m denotes the coefficient for the m th order component, and $M-1$ is the largest degree in the polynomial approximation. Hence, the expression for $Y[n]$ in (10) can be further approximated as

$$Y[n] \approx \sum_{i=0}^{I-1} \sum_{k=0}^{N_f-1} \left(\sum_{m=0}^{M-1} x_m n^m \right) u_{i,k}^n + W[n]. \quad (14)$$

The received signals expressed in (10) and (14) include the effects of the THz channel distortion, and will be used for the timing acquisition in the sequel LSR and ML algorithms, while not explicitly requiring the knowledge on the quantities $A_i[n]$ in (11). In general, by fitting the discrete frequency-domain of the received signal in (14) with a polynomial of a larger degree, we obtain better timing acquisition estimates. In our analysis, we select the degree of the polynomial estimation as $M = 20$ with a good approximation of the received waveforms.

B. Designing the Annihilating Filter

Next, in our LSR algorithm, we leverage the features of the annihilating filters which have been introduced in [14], [15] and apply them in the context of THz pulse-based communications. The key principle of utilizing the annihilating filter is to search for the zeros and the associated timing information. Based on the spectral coefficients, we proceed with designing the annihilating filter, $H_a[m]$. The N spectral coefficients $Y[n]$ are computed according to (14), with $N \geq 2L + 1$. The annihilating filter is

designed for guaranteeing

$$H_a[n] * Y[n] = \sum_{l=0}^L H_a[l] Y[n-l] \\ = 0, \text{ for } n = 0, 1, \dots, N-1, \quad (15)$$

where $L = I \cdot N_f \cdot M$. By exploiting the z -transform properties, the transfer function $H_a(z)$ in the z -domain is

$$H_a(z) = \sum_{l=0}^L H_a[l] z^{-l} \\ = \prod_{i=0}^{I-1} \prod_{k=0}^{N_f-1} [1 - z_{i,k}^0 z^{-1}]^M, \quad (16)$$

where $z_{i,k}^0$ denotes the zero of $H_a(z)$, and is a function of the frequency step f_0 as

$$z_{i,k}^0 = \exp(-j2\pi f_0 T_f (iN_f + k + \mu_i) - j2\pi f_0 T_s \nu_i) \\ = (u_{i,k}^n \cdot \exp(j2\pi f_L (T_f (iN_f + k + \mu_i) + T_s \nu_i)))^{\frac{1}{n}} \\ = \exp(-j2\pi f_0 (T_f (iN_f + k + \mu_i) + T_s \nu_i)). \quad (17)$$

The proof of the annihilating filter properties by combining (15), (16) and (17) is provided here. We expand the expression for $Y[n]$ according to (14) with high SNR,

$$H_a[n] * Y[n] = \sum_{l=0}^L H_a[l] Y[n-l] \\ \approx \sum_{l=0}^L \sum_{i=0}^{I-1} \sum_{k=0}^{N_f-1} H_a[l] \left(\sum_{m=0}^{M-1} x_m (n-l)^m \right) u_{i,k}^{n-l} \\ = \sum_{m=0}^{M-1} \sum_{i=0}^{I-1} \sum_{k=0}^{N_f-1} x_m \sum_{l=0}^L H_a[l] (n-l)^m u_{i,k}^{-l} u_{i,k}^n \\ = \sum_{m=0}^{M-1} \sum_{i=0}^{I-1} \sum_{k=0}^{N_f-1} x_m \cdot 0 \cdot u_{i,k}^n \\ = 0, \text{ for } n = 0, 1, \dots, N-1, \quad (18)$$

where we use the proposition $\sum_{l=0}^L H_a[l] (n-l)^m u_{i,k}^{-l} = 0$ in the Appendix in [11].

Our aim is to explore the properties of the annihilating filter to solve for the timing offsets. The annihilating filter has the degree of L with $L+1$ unknown filter coefficients, which consequently requires $L+1$ linear equations to solve for these annihilating filter coefficients. This suggests that $N \geq 2L+1$ samples are needed in $Y[n]$. The matrix form of (15) is

$$\begin{pmatrix} Y[L] & Y[L-1] & \cdots & Y[0] \\ Y[L+1] & Y[L] & \cdots & Y[1] \\ \vdots & \vdots & \ddots & \vdots \\ Y[2L] & Y[2L-1] & \cdots & Y[L] \end{pmatrix} \begin{pmatrix} H_a[0] \\ H_a[1] \\ \vdots \\ H_a[L] \end{pmatrix} = \mathbf{0}. \quad (19)$$

To efficiently solve for the annihilating filter coefficients, we can set $H_a[0] = 1$, without loss of generality. Then, the matrix

equation can be rearranged as

$$\mathbf{Y}' \cdot \mathbf{H}'_a = -\mathbf{Y}_1, \quad (20)$$

$$\mathbf{Y}' = \begin{pmatrix} Y[L-1] & Y[L-2] & \cdots & Y[0] \\ Y[L] & Y[L-1] & \cdots & Y[1] \\ \vdots & \vdots & \ddots & \vdots \\ Y[2L-1] & Y[2L-2] & \cdots & Y[L] \end{pmatrix}, \quad (21)$$

$$\mathbf{H}'_a = (H_a[1] \ H_a[2] \ \cdots \ H_a[L])^T, \quad (22)$$

$$\mathbf{Y}_1 = (Y[L] \ Y[L+1] \ \cdots \ Y[2L])^T, \quad (23)$$

and $(\cdot)^T$ denotes the transpose operator.

C. Determining the Timing Offsets

Next, we utilize the above derivations to compute the timing offsets. With the filter coefficients $H_a[m]$, the values of μ_i and ν_i can be estimated by exploiting the properties of the annihilating filter. After transforming the annihilating filter impulse response into the z -domain in (16), we relate the filter characteristics to the desired timing offsets. We take the approach to estimate the ST offset before the FT offset, which is reasonable since the ST offset contributes more significantly to the overall offset estimate. By denoting the estimated zeros as $\{\hat{z}_{i,k}^0\}$, the estimated ST offset is solved as

$$\hat{\mu}_i = \left[\frac{\sum_{k=0}^{N_f-1} \angle \hat{z}_{i,k}^0}{-2\pi f_0 T_f N_f} \right] - iN_f - \left[\frac{N_f - 1}{2} \right], \\ = \left[\frac{N_f (iN_f + \hat{\mu}_i) T_f + N_f T_s \hat{\nu}_i + \frac{N_f (N_f - 1) T_f}{2}}{T_f N_f} \right] \\ - iN_f - \left[\frac{N_f - 1}{2} \right], \\ = \left[iN_f + \hat{\mu}_i + \frac{(N_f - 1)}{2} + \frac{T_s \hat{\nu}_i}{T_f} \right] - iN_f - \left[\frac{N_f - 1}{2} \right] \quad (24)$$

where $\lfloor \cdot \rfloor$ denotes the floor operator, and $\hat{\nu}_i < Q$ is known. Moreover, a sum operation is performed on the angles of the estimated zeros that belong to the same symbol, i.e., $\sum_{k=0}^{N_f-1} \angle \hat{z}_{i,k}^0$. As shown in the THz transmission model in Fig. 2, the timing offset of each pulse within a symbol equals $(\tau_0 + t_D + \psi_i)$, which is independent of k . However, due to the noise effects and the THz channel distortion, the timing offset for the pulses within one symbol might become different. Therefore, we need to jointly consider the N_f pulses of one symbol in (24) to improve the accuracy of the timing offset estimation. By considering $\hat{\nu}_i < Q$, an accurate estimate of μ_i can be obtained in (24). Then, based on the estimated ST offset, the estimated FT

offset is

$$\begin{aligned} \hat{\nu}_i &= \left[\frac{\sum_{k=0}^{N_f-1} \angle \hat{z}_{i,k}^0}{-2\pi f_0 T_s N_f} \right] - Q \left(iN_f + \frac{N_f - 1}{2} + \hat{\mu}_i \right) \\ &= \left[\frac{(iN_f + \hat{\mu}_i) Q T_s + T_s \hat{\nu}_i + \frac{Q T_s (N_f - 1)}{2}}{T_s} \right] \\ &\quad - Q \left(iN_f + \frac{N_f - 1}{2} + \hat{\mu}_i \right). \end{aligned} \quad (25)$$

For (24) and (25), we search for the zeros $\hat{z}_{i,k}^0$ that are closest to the unit circle [11]. This algorithm is reliable when the noise level is low and the antenna gains are high. In THz band communications, beamforming techniques [3] as well as the pulse combining gain in (3) can effectively improve the SNR and hence decrease noise effects. Nevertheless, the problem of numerical ill-conditioning [12] may arise by using this approach, mainly because the root-finding is not robust to the noise effects. Alternatively, instead of finding the roots, the matrix manipulations can be performed, via exploiting the properties of the signal subspace [14], [29]. However, a major computational cost for this method arises in the singular value decomposition procedure of the matrix manipulations, which is not favored in this work.

V. MAXIMUM-LIKELIHOOD-BASED TIMING ACQUISITION APPROACH

The LSR algorithm developed in the previous section allows choosing a sub-Nyquist sampling rate and achieves good timing acquisition performance when the SNR is high. As a complementary approach, for the low SNR case (i.e., less than 10 dB), the ML criterion that are used in [17]–[19] is adopted to derive the timing acquisition solutions for the pulse-based THz band communication. A two-step approach involving the weighted construction method is utilized, where an overview of the ML approach is illustrated in Fig. 4.

A. ML Objective Function

Starting from the THz communication models in (4) and (6), we define a vector of the trial values of the unknown timing

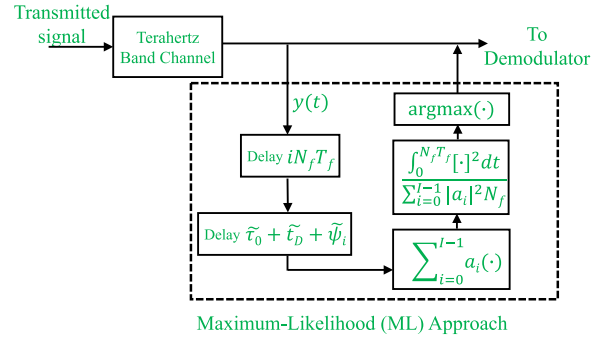


Fig. 4. Block diagram of the ML approach.

offsets as $(\tilde{\tau}_0, \tilde{\tau}_D, \tilde{\psi}_i)^T$. We describe $\tilde{z}(t)$ as the noise-free component of the trial received signal, as

$$\tilde{z}(t) = \sqrt{P_t} \sum_{i=0}^{I-1} a_i \sum_{k=0}^{N_f-1} \tilde{g}(t - iN_f T_f - kT_f - \tilde{\tau}_0 - \tilde{\tau}_D - \tilde{\psi}_i). \quad (26)$$

where $\tilde{g}(t)$ refers to the hypothetical channel-dependent received pulse. Then, the ML rule is applied to search $(\tilde{\tau}_0, \tilde{\tau}_D, \tilde{\psi}_i)^T$ and $\tilde{g}_1(t)$ for minimizing the integral of the squared magnitude of the difference signal $\int_t (y(t) - \tilde{z}(t))^2 dt$, which equivalently maximizes the expression in (27) shown at the bottom of this page, where we define $\tilde{g}_1(t) = \sum_{k=0}^{N_f-1} \tilde{g}(t - kT_f)$.

To further derive this objective function, we consider that the training symbols a_i defined in (3) are uncorrelated with each other. Moreover, according to the THz pulse modulation described in Section III-B, one symbol waveform is confined with the non-zero support over $[0, N_f T_f]$. Therefore, the objective function can be rearranged as (28) shown at the bottom of this page.

B. Two-Step Approach

The ML-based time acquisition problem can be solved by adopting a two-step procedure. In particular, the objective

$$\begin{aligned} \Lambda \left[y(t) \mid (\tilde{\tau}_0, \tilde{\tau}_D, \tilde{\psi}_i)^T, \tilde{g}_1(t) \right] &= 2 \int_0^{IN_f T_f} y(t) \tilde{z}(t) dt - \int_0^{IN_f T_f} [\tilde{z}(t)]^2 dt \\ &= 2 \int_0^{IN_f T_f} y(t) \sqrt{P_t} \sum_{i=0}^{I-1} a_i \tilde{g}_1(t - iN_f T_f - \tilde{\tau}_0 - \tilde{\tau}_D - \tilde{\psi}_i) dt - \int_0^{IN_f T_f} \left[\sqrt{P_t} \sum_{i=0}^{I-1} a_i \tilde{g}_1(t - iN_f T_f - \tilde{\tau}_0 - \tilde{\tau}_D - \tilde{\psi}_i) \right]^2 dt, \end{aligned} \quad (27)$$

$$\begin{aligned} \Lambda \left[y(t) \mid (\tilde{\tau}_0, \tilde{\tau}_D, \tilde{\psi}_i)^T, \tilde{g}_1(t) \right] &\approx 2\sqrt{P_t} \sum_{i=0}^{I-1} a_i \int_0^{N_f T_f} y(t + iN_f T_f + \tilde{\tau}_0 + \tilde{\tau}_D + \tilde{\psi}_i) \cdot \sum_{k=0}^{N_f-1} \tilde{g}(t - kT_f) dt - P_t \sum_{i=0}^{I-1} |a_i|^2 \int_0^{N_f T_f} \left[\sum_{k=0}^{N_f-1} \tilde{g}(t - kT_f) \right]^2 dt \\ &\approx 2\sqrt{P_t} \sum_{i=0}^{I-1} a_i \int_0^{N_f T_f} \tilde{g}_1(t) \cdot y(t + iN_f T_f + \tilde{\tau}_0 + \tilde{\tau}_D + \tilde{\psi}_i) dt - P_t \sum_{i=0}^{I-1} |a_i|^2 \int_0^{N_f T_f} [\tilde{g}_1(t)]^2 dt. \end{aligned} \quad (28)$$

function can be written by taking $\tilde{g}_1(t)$ as a nuisance, as

$$\begin{aligned} & (\tilde{\tau}_0 + \tilde{t}_D + \tilde{\psi}_i) \\ & = \arg \max_{\tilde{g}_1(t)} \left\{ \max_{\tilde{g}_1(t)} \left\{ \Lambda \left[y(t) \mid \left(\tilde{\tau}_0, \tilde{t}_D, \tilde{\psi}_i \right)^T, \tilde{g}_1(t) \right] \right\} \right\}, \end{aligned} \quad (29)$$

where the overall timing offset information (i.e., $\tilde{\theta} = \tilde{\tau}_0 + \tilde{t}_D + \tilde{\psi}_i$) is estimated as the parameter of interest, instead of the individual ones. To solve the inner maximization in (29), we fix $(\tilde{\tau}_0, \tilde{t}_D, \tilde{\psi}_i)^T$ and set $\frac{\partial \Lambda}{\partial \tilde{g}_1(t)} = 0$ in (28) with t confined over $[0, N_f T_f]$. The resulting optimal estimate of the received pulse waveform $\tilde{g}_1(t)$ is

$$\begin{aligned} \tilde{g}_1(t) &= \frac{1}{\sum_{i=0}^{I-1} \sqrt{P_t} |a_i|^2 N_f} \\ & \cdot \sum_{i=0}^{I-1} a_i y(t + i N_f T_f + \tilde{\tau}_0 + \tilde{t}_D + \tilde{\psi}_i). \end{aligned} \quad (30)$$

This estimate can be interpreted as the weighted construction with the normalized known training symbols $\frac{a_i}{\sum_{i=0}^{I-1} |a_i|^2}$ as the weighting coefficients. By substituting (30) into (28) and (29), we obtain the solution to the timing acquisition problem. As a result, the timing offset is given by (31) shown at the bottom of this page, which is equivalent to maximize the energy.

The cost of the ML approach is affected by the size of the search space, and can be reduced by enlarging the time step for searching. In the ML algorithm, the time step is defined as the multiples of the Nyquist sampling interval $T_{ny} = 1/N_{ny}$. However, the increase of the time step will degrade the acquisition performance of the ML algorithm. The tradeoff between the synchronization performance and the complexity is numerically investigated in Section VII.

VI. ERROR ANALYSIS

The proposed timing acquisition schemes are evaluated by using the metric of the root-mean-square-error (RMSE). A lower RMSE requires a smaller LSR factor in the LSR algorithm or a small time step in the ML scheme. In this section, we first provide an estimation error analysis in terms of the RMSE and the CRLB both analytically and numerically. Then, we derive an analytical expression of the BER as a function of the timing acquisition errors.

A. Root-Mean-Square-Error (RMSE) and Cramer-Rao Lower Bound (CRLB)

To evaluate the developed algorithms, we analyze the RMSE of timing estimates and compare with the CRLB. First, we define

the estimation error in the i th symbol of the signal as

$$\tilde{\epsilon}_i = (\tilde{\tau}_0 + \tilde{t}_D + \tilde{\psi}_i) - (\tau_0 + t_D + \psi_i). \quad (32)$$

Over the I symbols of the transmitted signal in (3), the normalized RMSE of the estimation error $\tilde{\epsilon}_i$ at the frame level is given by

$$\Psi = \frac{\sqrt{\frac{1}{I} \sum_{i=0}^{I-1} \tilde{\epsilon}_i^2}}{T_f} \quad (33)$$

1) *RMSE of LSR Algorithm:* To approximate the RMSE of the LSR algorithm by a function of the SNR, we employ an analytical expression developed via a first order perturbation analysis [31],

$$\begin{aligned} \Psi_{\text{LSR}} &\approx \sqrt{\frac{2M+1}{6(\pi f_0)^2 \cdot (N-M)^2 (M^2+M) \cdot \text{SNR}}} \\ &\approx \sqrt{\frac{1}{3M(\pi f_0)^2 \cdot N^2 \cdot \text{SNR}}}, \end{aligned} \quad (34)$$

where the approximation in (34) is a function of the frequency step f_0 , the polynomial degree M , and the total number N of frequency samples $Y[n]$ in (10).

2) *RMSE of ML Algorithm:* To approximate the RMSE of the ML algorithm, we make some relaxation assumptions. First, the overall timing offset information (i.e., $\theta = \tau_0 + t_D + \psi_i$ and $\tilde{\theta} = \tilde{\tau}_0 + \tilde{t}_D + \tilde{\psi}_i$) does not vary among different symbols. Then, the maximization in (31) could be performed with respect to a single parameter θ . Moreover, we ignore the presence of the noise.

Under the above assumptions, combining (31) and (4) yields

$$\begin{aligned} & \int_0^{N_f T_f} \left[\sum_{i=0}^{I-1} a_i y(t + i N_f T_f + \tilde{\tau}_0 + \tilde{t}_D + \tilde{\psi}_i) \right]^2 dt \\ & = P_t \sum_{i=0}^{I-1} \sum_{i'=0}^{I-1} \sum_{q=0}^{I-1} \sum_{q'=0}^{I-1} a_i a_{i'} a_q a_{q'} \int_0^{N_f T_f} A dt. \end{aligned} \quad (35)$$

$$\begin{aligned} A &= g_1 \left(t + (i - i') N_f T_f + \tilde{\theta} - \theta \right) \\ & \cdot g_1 \left(t + (q - q') N_f T_f + \tilde{\theta} - \theta \right) \end{aligned} \quad (36)$$

with $g_1(t) = \sum_{k=0}^{N_f-1} g(t - k T_f)$, analogously to the definition in (27). Inspection of (35) and (36) reveals that the maximum of the likelihood function is achieved over an interval of values, $\tilde{\theta} \in [\beta, \theta]$ with $\beta = \max\{0, \theta + T_g - T_f\}$. We denote T_g as the pulse width of the received pulse, which is smaller than T_f that is the frame duration, as defined in Section III-B. This could be

$$\begin{aligned} (\tilde{\tau}_0 + \tilde{t}_D + \tilde{\psi}_i) &= \arg \max \left\{ \frac{1}{\sum_{i=0}^{I-1} \sqrt{P_t} |a_i|^2 N_f} \int_0^{N_f T_f} \left[\sum_{i=0}^{I-1} a_i y(t + i N_f T_f + \tilde{\tau}_0 + \tilde{t}_D + \tilde{\psi}_i) \right]^2 dt \right\} \\ &= \arg \max \left\{ \int_0^{N_f T_f} \left[\sum_{i=0}^{I-1} a_i y(t + i N_f T_f + \tilde{\tau}_0 + \tilde{t}_D + \tilde{\psi}_i) \right]^2 dt \right\} \end{aligned} \quad (31)$$

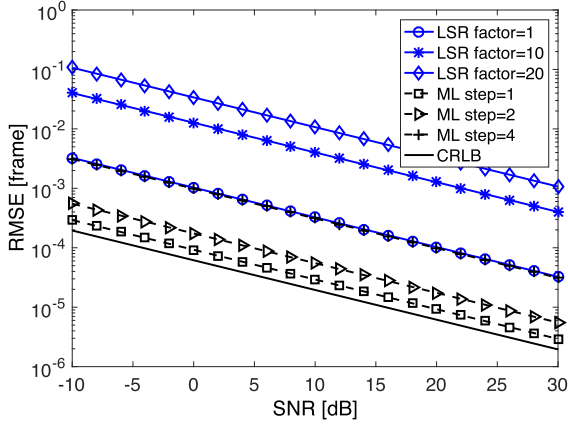


Fig. 5. Timing acquisition RMSE in comparison with the CRLB.

interpreted that $\tilde{\theta} \in [\beta, \theta]$ could maximize the likelihood function as long as the pulse with the estimated offset and the pulse with the true offset are incorporated within one frame duration. As a result, the RMSE of the ML algorithm is approximately given by

$$\Psi_{\text{ML}} \approx \sqrt{\frac{(\theta - \beta)^2}{3}}. \quad (37)$$

This reveals a gap between the performance of the ML method and the CRLB.

3) *CRLB*: By contrast, the CRLB suggests a lower bound on achievable RMSE for any unbiased estimation methods [32], as

$$\text{CRLB} \{\tilde{\epsilon}\} = \sqrt{\frac{3}{2(\pi f_0)^2 \cdot N^3 \cdot \text{SNR}}}. \quad (38)$$

The CRLB provides a theoretical bound on the performance of the proposed two algorithms. The estimation performance based on the ML estimator is lower-bounded by the CRLB, and deteriorates as the ML step increases between the SNR range of -10 dB to 30 dB. To compare the RMSE performance of the LSR algorithm with the CRLB in Fig. 5, the LSR algorithm provides a very good estimation performance. Moreover, the difference between the RMSE of the LSR algorithm and the CRLB decreases, as the polynomial degree is comparable to the number of frequency samples, i.e., $N \geq 2IN_fM + 1$, as described in Section IV-B. In particular, by increasing the sampling rate X times for the same SNR, the RMSE of the LSR algorithm decreases by a factor of $M^{1/2} \cdot X$, while the CRLB reduces by a greater factor of $X^{3/2}$ as can be deduced from (38).

As the LSR factor (β_{LSR} in Fig. 3) increases from 1 to 10 and 20, the performance difference between the LSR algorithm and the CRLB increases. At SNR = 30 dB, the approximated RMSEs are 3×10^{-5} , 4×10^{-4} and 1×10^{-3} respectively, while the CRLB or equivalently, the performance of the ML algorithm with a time step of 1, is equal to 2×10^{-6} . The RMSE performance becomes worse as the SNR decreases, and is further away from the CRLB as the LSR factor increases. Furthermore, by comparing with the simulation results, the approximations are in good agreements particularly for high SNR. In addition, the error performance of the ML method is studied, for different time steps ranging from 1, 2 to 4. The ML method generally outperforms the LSR approach.

TABLE I
PHYSICAL PARAMETERS USED IN THE SIMULATIONS

Symbol	Parameter	Value	Unit
T_{ny}	Nyquist sampling interval	0.5	ps
T_p	Pulse width	10	ps
T_f	Frame length	1	ns
I	Number of training symbols	[1, 2]	–
N_f	Number of frames for one symbol	[1, 4]	–
f_0	Frequency step	10	MHz
P_t	Transmit power	1	dBm
G_t	Transmit antenna gain	[0, 30]	dBi
G_r	Receive antenna gain	[0, 30]	dBi
P_w	Noise power	–80	dBm
f_L	Lower cutoff frequency	0.06	THz
f_U	Upper cutoff frequency	1	THz
d_T	Communication distance	[1, 20]	m

B. BER Sensitivity

In the following, we evaluate the BER performance of the THz receiver equipped with the above timing acquisition methods. The goal is to assess the BER sensitivity caused by the timing acquisition errors while assuming ideal channel estimation. Particularly for the pulse-based systems, by incorporating the noise effect, the complementary error function $\text{erfc}(\cdot)$ of the SNR was shown to capture the error behavior [33]–[35]. In light of the received signal in (4), the timing errors model in (6), and the SNR expression in (7), the BER is given by

$$\rho_i(\mu_i, \nu_i) = \frac{1}{2} \text{erfc} \left(\sqrt{\frac{G_t G_r P_t |h|^2 N_f R_p^2 (\mu_i T_f + \nu_i T_s)}{2P_w}} \right), \quad (39)$$

where we consider a_i takes a value from $\{+1, -1\}$ with equal probabilities. In (39), $R_p(t)$ describes the normalized auto-correlation function of the THz pulse, $p(t)$, given in (3), as

$$R_p(\tau) = A_R \int_{-\infty}^{+\infty} p(t)p(t-\tau)dt, \quad (40)$$

where A_R is the normalizing factor. If the timing acquisition is perfect, the best-case BER is equal to

$$\rho_i(0, 0) = \frac{1}{2} \text{erfc} \left(\sqrt{\frac{G_t G_r P_t |h|^2 N_f}{2P_w}} \right), \quad (41)$$

where the term inside the complementary error function is the square root of the SNR dividing by a scalar of 2. In the above equation, the BER decreases for higher SNR, smaller timing acquisition errors, and larger number of pulses per symbol.

VII. PERFORMANCE EVALUATION

In this section, we assess the LSR synchronization algorithm and the ML-based approach in terms of the timing offset estimation performance, based on Monte Carlo simulations. All presented results are averages over 1000 realizations. Moreover, we study the influence of synchronization on the resulting received signals. Finally, we analyze the BER sensitivity as a function of the timing acquisition errors for the two algorithms. We consider the following choice of parameters in the simula-

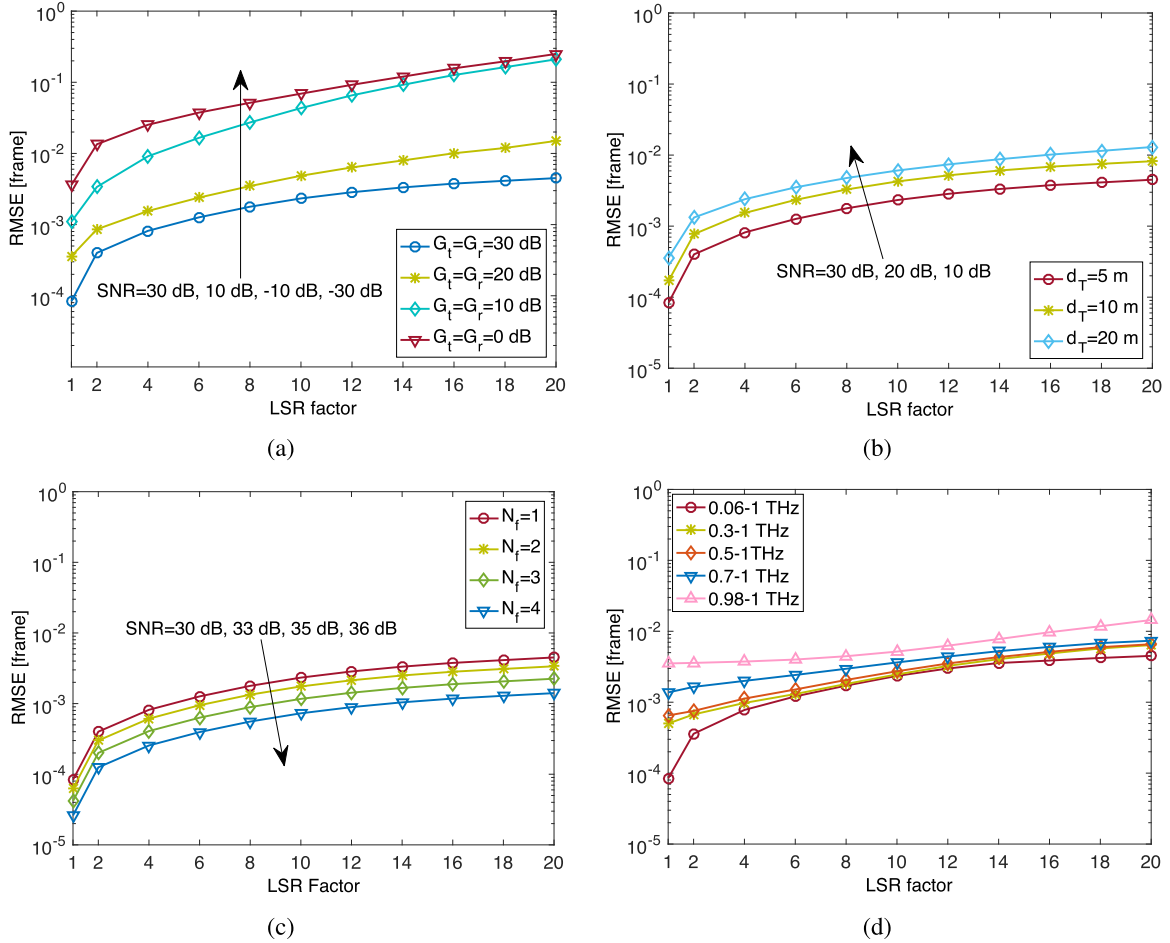


Fig. 6. RMSE of the LSR algorithm for different THz-band physical parameters. (a) RMSE for different antenna gains, with $d_T = 5$ m and $N_f = 1$. (b) RMSE for different distances, with $G_t = G_r = 30$ dB and $N_f = 1$. (c) RMSE for different number of pulses per symbol, which relates to the symbol rates, by considering $G_t = G_r = 30$ dB and $d_T = 1$. (d) RMSE for different pulse widths in the frequency domain.

tions. The random initial delay τ_0 and the random misalignment between the transmitter and the receiver ψ_i in (6) follow uniform distributions over $[-T_f, T_f]$, and are multiples of $T_{ny} = 0.5$ ps. The physical parameters that are used in the simulations unless otherwise stated are listed in Table I [28].

Computational complexity: A major computational load of the LSR algorithm is associated with the matrix manipulation in (19), with the computational complexity of order $\mathcal{O}(N^3)$, where N denotes the total number of frequency samples $Y[n]$ in (10) used in the LSR algorithm. By contrast, the ML-based approach requires $\mathcal{O}(N_n^2)$ operations, where N_n denotes the number of samples taken at the Nyquist rate N_{ny} .

A. LSR Algorithm Performance

In the following, timing offset estimation based on the LSR algorithm developed in Section IV is considered. After determining the filter coefficients, we can find the roots in the z -domain. Based on the results of roots finding, we obtain the timing offset. We study the RMSE as a function of the LSR factor, for different antenna gains, distances, pulse waveforms and transmission bands. As our main objective is to achieve an accurate synchronization by using a sub-Nyquist sampling rate, we investigate which LSR factors β_{LSR} can support $\text{RMSE} \leq 0.01T_f$. The results and the observations are discussed as follows.

1) **Impact of Antenna Gain:** In Fig. 6(a), the RMSE performance is evaluated for different antenna gains. In particular, when the antenna gains equal $G_t = G_r = 30$ dB by benefiting from the very large antenna arrays, and the communication distance is $d_T = 5$ m in (2), $\beta_{LSR} = 20$ can be adopted. In this case, the path loss is approximately 110 dB [27] and the resulting SNR is equal to 30 dB. On the one hand, a reduction of antenna gains implies a decrease in SNR, which makes RMSE increasing significantly. As the antenna gains are equal to 20 dB, 10 dB and 0 dB, the maximum LSR factor reduces from 16 to 4 and 2. With these antenna gains, the SNR values reduce to 10 dB, -10 dB, and -30 dB. At the Nyquist sampling rate, the RMSE increases to 3×10^{-4} , 1×10^{-3} and 3×10^{-3} , respectively. These results are consistent with the analytical studies in Section VI-A for the high SNR values, i.e., larger than 10 dB. For lower SNR values, the analytical expression in (34) overestimates the RMSE, i.e., the analytical expressions yield larger RMSE values than the simulations. Hence, when the antenna gains or the equivalent SNR are very small, the RMSE becomes significant and the LSR algorithm is not suitable to be used.

2) **Impact of Communication Distance:** Moreover, we study the influence of communication distances on the synchronization performance in Fig. 6(b). In general, as the distance increases, a higher path loss results and more severe frequency-selectivity appears in the THz band spectrum. This

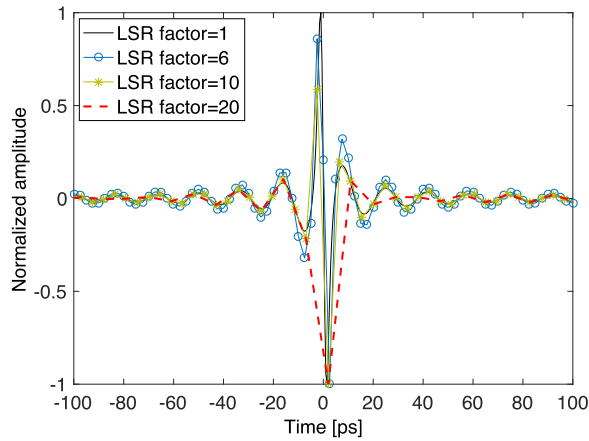


Fig. 7. Sampled signals for different LSR factors.

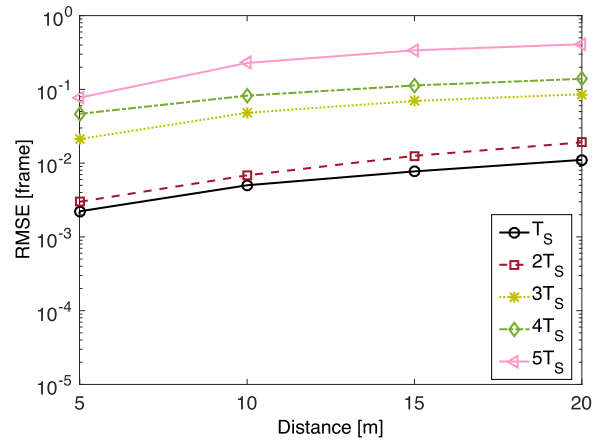
consequently degrades the RMSE of the LSR algorithm. Although the LSR factor $\beta_{\text{LSR}} = 20$ can be supported to achieve $\text{RMSE} = 0.01$ frame, the average RMSE values increase from 0.003, 0.005, 0.007 to 0.011, as the distance increases from 5 m, 10 m, to 20 m. At these distances, the SNR values are equal to 30 dB, 20 dB and 10 dB.

3) *Impact of Pulse Repetitions*: In addition, the influence of the number of the pulses to represent one symbol (N_f) in (3) is studied in Fig. 6(c). The increase of the number of pulses per symbol N_f leads to the improvement of the SNR of $10 \log_{10}(N_f)$ dB, which results in a reduced RMSE. For all N_f , the LSR factor of 20 can be supported for $d = 5$ m and $G_t = G_r = 30$ dB. The possibility of an increase of the number of frames is important when a targeted SNR is mandatory while the antenna gains and the transmit power are fixed, as shown in (7). Moreover, the BER decreases for a larger number of pulses per symbol as suggested in Section VI-B. However, this is at the cost of the reduction of the data rate by a factor of N_f .

4) *Impact of Pulse Width*: The effect of five pulses with different bandwidths is shown in Fig. 6(d). With a very small pulse duration T_p , the supporting bandwidth is large, which yields a better performance of the LSR algorithm. This can be explained by the fact that with the wider frequency response, there are more available frequency samples for the LSR algorithm, for a given LSR factor and reference sampling rate, e.g., 2 THz in our simulations. In particular, a 10 ps pulse has a frequency response occupying the spectrum between 0.06 and 1 THz. This pulse waveform is able to support an RMSE of 0.01 frame with an LSR factor of 20. The observations would be different if the reference sampling rate is equal to the true Nyquist rate that varies with the pulse width and the supporting bandwidth.

B. Influence on Received Signal

We analyze the effect of the LSR algorithm on the received signal for different LSR factors in Fig. 7, with $N_f = 1$. With smaller sampling rates, the recovery of the received signal becomes more challenging. The RMSE values between the received pulse with $\beta_{\text{LSR}} = 1$ and the received pulses at sub-Nyquist sampling rates are evaluated in the time domain, which increases from 1.26×10^{-3} , 2.33×10^{-3} to 4.50×10^{-3} , when $\beta_{\text{LSR}} = 6, 10$ and 20. Although the recovery of received signals becomes challenging, the transmitted symbols can still be detected based on the signal power available for pulse-based

Fig. 8. RMSE of the ML algorithm for different time steps, with $G_t = G_r = 0$ dB.

communication in the THz band. The received pulses experience severe distortion in the THz band channel.

In addition to the amplitude and phase distortion, temporal broadening effects appear, due to the very high frequency-selectivity in the wideband THz spectrum [3]. The width of the received pulse independent of β_{LSR} is over 200 ps, which is 20 times larger than the transmitted pulse. However, by using a low sampling rate, the rapid fluctuation in the received pulses dwindles, and hence, the broadening effects attenuate. For example, when the LSR factors are 10 and 20, the width of the received pulse reduces to 180 ps and 150 ps, respectively. These are equivalent to suggest the maximal pulse rates of 5.56 and 6.67 Giga-pulses-per-second to avoid the inter-symbol-interference. The details on the temporal broadening effect and its influences on received pulses can be found in [5]. Hence, the LSR algorithm can effectively relax the restriction of the minimum spacing between consecutive pulse transmissions. However, the signal fluctuation still exists even by sparse sampling at a low-sampling rate. By considering the closely spaced consecutive pulses, the fluctuation amplifies and the inter-pulse interference might still occur. Therefore, the spacing between consecutive pulse transmissions needs further studies with the sub-Nyquist sampling.

C. ML Approach Performance

The LSR algorithm is not favored when the SNR at the receiver is low, for example in the multipath propagation [5], or with $G_t = G_r = 0$ dB in (2). As an alternative, the ML approach yields better performance than the LSR algorithm, at the cost of significant search space and data storage. The RMSE performance of the ML-based approach is shown in Fig. 8. These results match with the observations in Section VI-A. As a major computational constraint, different time step values (multiples of the Nyquist sampling interval T_{ny}) of the trial values in (31) are studied. The RMSE increases when the distance increases and the search space decreases. To achieve $\text{RMSE} = 0.01$ frame, a time step of 2 can be used to reduce the search space by half. However, the distance needs to remain below 15m. Specifically at $d_T = 5$ m, the RMSE increases from 0.002, 0.003, 0.021, 0.046 to 0.077 when the time step increases from 1 to 5, respectively. For $d_T = 5$ m, the SNR is equal to -30 dB, and $\text{CRLB} = 1.9 \times 10^{-3}$, which lower-bounds the RMSE of the

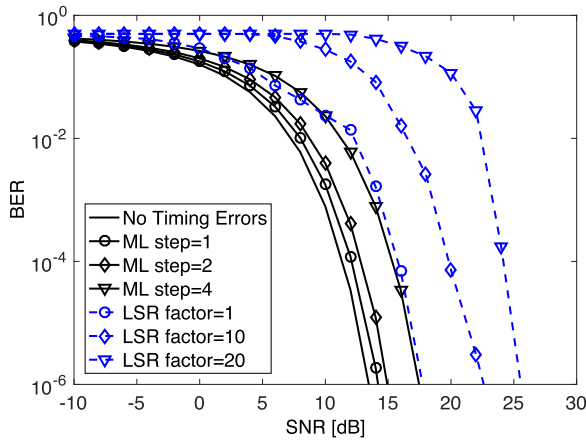


Fig. 9. BER sensitivity for the LSR and ML algorithms.

ML method. Hence, the ML-based algorithm can be used when the SNR is low, with a time step of 2 to reduce the search space by half.

Furthermore, the timing estimate based on the ML algorithm is computed after collecting all the training symbols according to (31). Therefore, as determined by the pulse-based transmission scheme, the accuracy of the timing estimate is at an order of ten picoseconds. However, the computing duration for timing acquisition based on the ML algorithm is at an order of nanoseconds. In terms of mobility, we have the following considerations. Assuming a vehicle speed of 100 km/h and a computation time of the algorithm of a few nanoseconds, the vehicle has moved less than 1 micrometers until convergence. Since the typical wavelengths in THz communications are 100 micrometers and more, initial acquisition should have no problems. However, on the other hand, tracking is a different issue, but one could even repeat the ML algorithm periodically for this in a first approach.

D. BER Sensitivity

The BER sensitivity is given in (39), where μ_i is of the order of the frame length, T_f , while ν_i is of the order of the sampling interval, T_s , as defined in (6). The BER sensitivity is presented in Fig. 9 for the different timing acquisition methods and parameters. The curve corresponding to the ideal timing acquisition in (41) provides a benchmark to quantify the performance loss due to timing acquisition errors. The results appear to be consistent with the aforementioned RMSE performance of the algorithms. Indeed, like the RMSE, the BER performance degrades as the ML step size increases and as the LSR factor increases. Moreover, the LSR algorithm shows a larger performance loss compared to the ML method, particularly at SNR smaller than 18 dB. Hence, the LSR algorithm is recommended for directional transmission while the ML method is suitable at low SNR as a complementary.

VIII. CONCLUSION

In this paper, we have proposed and analyzed the LSR and the ML-based algorithms for timing acquisition in the THz band to address the challenges such as the THz band channel peculiarities and the ultra-high sampling rate demand. The error performance of the algorithms has been analytically approximated, where the results have shown good agreements with the

simulation results when the SNR is high. Moreover, we have analytically and numerically evaluated the two timing acquisition algorithms, in comparison with the CRLB. Furthermore, we have studied the BER sensitivity to the acquisition errors in the two algorithms. With the metric of the RMSE, the simulation results showed that the timing accuracy at an order of ten picoseconds is achievable. In particular, when the SNR is high (i.e., greater than 18 dB benefiting from high gain antennas), the LSR algorithm can be used with the uniform sampling at $1/20$ of the Nyquist rate, while the ML-based algorithm can be used for low SNR with a time step of 2 to reduce the search space by half. The LSR algorithm can also effectively mitigate the temporal broadening effect due to the frequency-selectivity of the THz channel. This work contributes to achieving a reliable timing acquisition with a reduced sampling rate for digital transmissions in the THz band. The developed synchronization solutions could be included as part of a receiver design.

REFERENCES

- [1] H. Song and T. Nagatsuma, "Present and future of Terahertz communications," *IEEE Trans. THz Sci. Technol.*, vol. 1, no. 1, pp. 256–263, Sep. 2011.
- [2] T. Kleine-Ostmann and T. Nagatsuma, "A review on Terahertz communications research," *J. Infrared, Millim. THz Waves*, vol. 32, pp. 143–171, 2011.
- [3] I. F. Akyildiz, J. M. Jornet, and C. Han, "Terahertz band: Next frontier for wireless communications," *Phys. Commun. J.*, vol. 12, pp. 16–32, 2014.
- [4] I. F. Akyildiz, J. M. Jornet, and C. Han, "Teranets: Ultra-broadband communication networks in the Terahertz band," *IEEE Wireless Commun. Mag.*, vol. 21, no. 4, pp. 130–135, Aug. 2014.
- [5] C. Han, A. O. Bicen, and I. F. Akyildiz, "Multi-ray channel modeling and wideband characterization for wireless communications in the Terahertz band," *IEEE Trans. Wireless Commun.*, vol. 14, no. 5, pp. 2402–2412, May 2015.
- [6] J. Y. Lee and R. A. Scholtz, "Ranging in a dense multipath environment using an UWB radio link," *IEEE J. Sel. Areas Commun.*, vol. 20, no. 9, pp. 1677–1683, Dec. 2002.
- [7] S. R. Aedudodla, S. Vijayakumaran, and T. F. Wong, "Timing acquisition in ultra-wideband communication systems," *IEEE Trans. Veh. Technol.*, vol. 54, no. 5, pp. 1570–1583, Sep. 2005.
- [8] Q. Liu, Y. Wang, and A. E. Fathy, "A compact integrated 100 Gs/s sampling module for UWB see through wall radar with fast refresh rate for dynamic real time imaging," in *Proc. IEEE Radio Wireless Symp.*, 2012, pp. 59–62.
- [9] C. H. Sarantos and N. Dagli, "A photonic analog-to-digital converter based on an unbalanced Mach-Zehnder quantizer," *Opt. Express*, vol. 18, no. 14, pp. 14598–14603, 2010.
- [10] R. G. Baraniuk, E. Candès, R. Nowak, and M. Vetterli, "Compressive sampling," *IEEE Signal Process. Mag.*, vol. 25, no. 2, pp. 12–13, Mar. 2008.
- [11] M. Vetterli, P. Marziliano, and T. Blu, "Sampling signals with finite rate of innovation," *IEEE Trans. Signal Process.*, vol. 50, no. 6, pp. 1417–1428, Jun. 2002.
- [12] I. Maravic and M. Vetterli, "Sampling and reconstruction of signals with finite rate of innovation in the presence of noise," *IEEE Trans. Signal Process.*, vol. 53, no. 8, pp. 2788–2805, Aug. 2005.
- [13] J. Kusuma, A. Ridolfi, and M. Vetterli, "Sampling of communication systems with bandwidth expansion," in *Proc. IEEE Int. Conf. Commun.*, 2002, vol. 3, pp. 1601–1605.
- [14] V. Y. Tan and V. K. Goyal, "Estimating signals with finite rate of innovation from noisy samples: A stochastic algorithm," *IEEE Trans. Signal Process.*, vol. 56, no. 10, pp. 5135–5146, Oct. 2008.
- [15] P. Shukla and P. L. Dragotti, "Sampling schemes for multidimensional signals with finite rate of innovation," *IEEE Trans. Signal Process.*, vol. 55, no. 7, pp. 3670–3686, Jul. 2007.
- [16] C. Han, I. F. Akyildiz, and W. H. Gerstacker, "Timing acquisition for pulse-based wireless systems in the Terahertz band," in *Proc. 2nd Annu. Int. Conf. Nanoscale Comput. Commun.*, pp. 7–12, Sep. 2015.
- [17] A. J. Coulson, "Maximum likelihood synchronization for OFDM using a pilot symbol: Algorithms," *IEEE J. Sel. Areas Commun.*, vol. 19, no. 12, pp. 2486–2494, Dec. 2001.

- [18] U. Mengali, *Synchronization Techniques for Digital Receivers*. Berlin, Germany: Springer, 2013.
- [19] C. Carbonelli and U. Mengali, "Synchronization algorithms for UWB signals," *IEEE Trans. Commun.*, vol. 54, no. 2, pp. 329–338, Feb. 2006.
- [20] R. G. Cid-Fuentes, J. M. Jornet, I. F. Akyildiz, and E. Alarcón, "A receiver architecture for pulse-based electromagnetic nanonetworks in the Terahertz band," in *Proc. IEEE Int. Conf. Commun.*, 2012, pp. 4937–4942.
- [21] A. Gupta, M. Medley, and J. M. Jornet, "Joint synchronization and symbol detection design for pulse-based communications in the THz band," in *Proc. IEEE Globecom*, 2015, pp. 1–7.
- [22] J. Kusuma, I. Maravić, and M. Vetterli, "Sampling with finite rate of innovation: Channel and timing estimation for UWB and GPS," in *Proc. IEEE Int. Conf. Commun.*, 2003, pp. 3540–3544.
- [23] A. A. D'amico, U. Mengali, and L. Taponecco, "Energy-based TOA estimation," *IEEE Trans. Wireless Commun.*, vol. 7, no. 3, pp. 838–847, Mar. 2008.
- [24] M. Flury, R. Merz, and J.-Y. Le Boudec, "Synchronization for impulse-radio UWB with energy-detection and multi-user interference: Algorithms and application to IEEE 802.15.4a," *IEEE Trans. Signal Process.*, vol. 59, no. 11, pp. 5458–5472, Nov. 2011.
- [25] I. Maravic, J. Kusuma, and M. Vetterli, "Low-sampling rate UWB channel characterization and synchronization," *IEEE J. Commun. Netw.*, vol. 5, no. 4, pp. 319–327, Dec. 2003.
- [26] N. Kurosawa, H. Kobayashi, K. Maruyama, H. Sugawara, and K. Kobayashi, "Explicit analysis of channel mismatch effects in time-interleaved ADC systems," *IEEE Trans. Circuits Syst. I, Fundam. Theory Appl.*, vol. 48, no. 3, pp. 261–271, Mar. 2001.
- [27] J. M. Jornet and I. F. Akyildiz, "Channel modeling and capacity analysis for electromagnetic wireless nanonetworks in the Terahertz band," *IEEE Trans. Wireless Commun.*, vol. 10, no. 10, pp. 3211–3221, Oct. 2011.
- [28] C. Han, A. O. Bicen, and I. F. Akyildiz, "Multi-wideband waveform design for distance-adaptive wireless communications in the Terahertz band," *IEEE Trans. Signal Process.*, vol. 64, no. 4, pp. 901–922, Feb. 2016.
- [29] H. A. Asl, P. L. Dragotti, and L. Baboulaz, "Multichannel sampling of signals with finite rate of innovation," *IEEE Signal Process. Lett.*, vol. 17, no. 8, pp. 762–765, Aug. 2010.
- [30] I. Maravić and M. Vetterli, "Exact sampling results for some classes of parametric nonbandlimited 2-D signals," *IEEE Trans. Signal Process.*, vol. 52, no. 1, pp. 175–189, Jan. 2004.
- [31] Y. Hua and T. K. Sarkar, "Matrix pencil method for estimating parameters of exponentially damped/undamped sinusoids in noise," *IEEE Trans. Acoust., Speech Signal Process.*, vol. 38, no. 5, pp. 814–824, May 1990.
- [32] H. Miao, K. Yu, and M. J. Juntti, "Positioning for NLOS propagation: Algorithm derivations and Cramer–Rao bounds," *IEEE Trans. Veh. Technol.*, vol. 56, no. 5, pp. 2568–2580, Sep. 2007.
- [33] S. Gezici, H. Kobayashi, H. V. Poor, and A. F. Molisch, "Performance evaluation of impulse radio UWB systems with pulse-based polarity randomization," *IEEE Trans. Signal Process.*, vol. 53, no. 7, pp. 2537–2549, Jul. 2005.
- [34] Z. Tian and G. B. Giannakis, "BER sensitivity to mistiming in ultrawideband impulse radios-part I: Nonrandom channels," *IEEE Trans. Signal Process.*, vol. 53, no. 4, pp. 1550–1560, Apr. 2005.
- [35] A. Rajeswaran, V. S. Somayazulu, and J. R. Foerster, "Rake performance for a pulse based UWB system in a realistic UWB indoor channel," in *Proc. IEEE Int. Conf. Commun.*, 2003, pp. 2879–2883.



Chong Han (M'16) received the Bachelor of Engineering degree in electrical engineering and telecommunications from The University of New South Wales, Sydney, NSW, Australia, in 2011, and the Master of Science and the Ph.D. degrees in electrical and computer engineering from the Georgia Institute of Technology, Atlanta, GA, USA, in 2012 and 2016, respectively. He is currently an Assistant Professor and Associate Special Research Fellow with the University of Michigan–Shanghai Jiao Tong University Joint Institute, Shanghai Jiao Tong University, Shanghai, China. Since 2017, he has been a collaborating Researcher with the Shenzhen Institute of Terahertz Technology and Innovation, Shenzhen, China. His current research interests include Terahertz band communication networks, 5G cellular networks, electromagnetic nanonetworks, and Graphene-enabled wireless communications.



Ian F. Akyildiz (M'86–SM'89–F'96) received the B.S., M.S., and Ph.D. degrees in computer engineering from the University of Erlangen-Nurnberg, Erlangen, Germany, in 1978, 1981, and 1984, respectively. He is currently the Ken Byers Chair Professor in Telecommunications in the School of Electrical and Computer Engineering, Georgia Institute of Technology, Atlanta, GA, USA, the Director of the Broadband Wireless Networking Laboratory, and the Chair of the Telecommunication Group at Georgia

Tech. He is an Honorary Professor in the School of Electrical Engineering, Universitat Politècnica de Catalunya, Barcelona, Spain, and founded the NaNoNetworking Center in Catalunya. Since September 2012, he has been a FiDiPro Professor (Finland Distinguished Professor Program supported by the Academy of Finland) in the Department of Communications Engineering, Tampere University of Technology, Tampere, Finland. His current research interests are in Terahertz band communication, nanonetworks, software defined networking, 5G cellular systems and wireless underground sensor networks. He is the Editor-in-Chief of *Computer Networks* (Elsevier) Journal, and the founding Editor-in-Chief of the *Ad Hoc Networks* (Elsevier) Journal, the *Physical Communication* (Elsevier) Journal, and the *Nano Communication Networks* (Elsevier) Journal. He is a Fellow of ACM (1997). He received numerous awards from IEEE and ACM.



Wolfgang H. Gerstacker (S'93–M'98–SM'11) received the Dipl.Ing. degree in electrical engineering from Friedrich-Alexander University Erlangen-Nrnberg, Erlangen, Germany, in 1991, the Dr.Ing. degree in 1998, and the Habilitation degree in 2004 from the same university.

Since 2002, he has been with the Institute for Digital Communications of the FAU Erlangen-Nrnberg, where he is currently a Professor. His research interests include the broad area of digital communications and statistical signal processing.

Dr. Gerstacker is an Editor for the IEEE TRANSACTIONS ON WIRELESS COMMUNICATIONS. He is an Area Editor for *Elsevier Physical Communication* and has been a Member of the Editorial Board of EURASIP JOURNAL ON WIRELESS COMMUNICATIONS AND NETWORKING. He has served as a Guest Editor for several Special Issues of and has been a Technical Program Co-Chair and the General Chair of several IEEE and ACM conferences. He received several awards including the Research Award of the German Society for Information Technology (2001), the IEEE/COM Innovation Award (2003), the Vodafone Innovation Award (2004), the Best Paper Award of EURASIP Signal Processing (2006), and the "Mobile Satellite & Positioning" Track Paper Award of VTC2011-Spring.